Available online at www.sciencedirect.com
SCIENCE DIRECT®
Journal of Computational Physics 204 (2005) 562–586
JOURNAL OF COMPUTATIONAL PHYSICS
www.elsevier.com/locate/jcp

Curvilinear parabolic approximation for surface wave transformation with wave–current interaction

Fengyan Shi *, James T. Kirby

Center for Applied Coastal Research, Center for Applied Coastal Research, University of Delaware, Newark, DE 19716, USA

Received 9 July 2004; received in revised form 15 October 2004; accepted 15 October 2004
Available online 19 November 2004

Abstract

The direct coordinate transformation method, which only transforms independent variables and retains Cartesian dependent variables, may not be an appropriate method for the purpose of simplifying the curvilinear parabolic approximation of the vector form of the wave–current equation given by Kirby [Higher-order approximations in the parabolic equation method for water waves, J. Geophys. Res. 91 (1986) 933–952]. In this paper, the covariant–contravariant tensor method is used for the curvilinear parabolic approximation. We use the covariant components of the wave number vector and contravariant components of the current velocity vector so that the derivation of the curvilinear equation closely follows the higher-order approximation in rectangular Cartesian coordinates in Kirby [Higher-order approximations in the parabolic equation method for water waves, J. Geophys. Res. 91 (1986) 933–952]. The resulting curvilinear equation can be easily implemented using the existing model structure and numerical schemes adopted in the Cartesian parabolic wave model [J.T. Kirby, R.A. Dalrymple, F. Shi, Combined Refraction/Diffraction Model REF/DIF 1, Version 2.6. Documentation and User's Manual, Research Report, Center for Applied Coastal Research, Department of Civil and Environmental Engineering, University of Delaware, Newark, 2004]. Several examples of wave simulations in curvilinear coordinate systems, including a case with wave–current interaction, are shown with comparisons to theoretical solutions or measurement data.

Keywords: Parabolic approximation; Curvilinear coordinates; Wave equations; Surface wave simulation; Wave–current interaction

1. Introduction

The parabolic equation method for water wave propagation has been known as effective means for predicting surface water waves over areas of variable bathymetry, including both the effects of refraction and

* Corresponding author. Fax: +1 302 831 1228.
E-mail address: fyshi@coastal.udel.edu (F. Shi).

0021-9991/$ - see front matter © 2004 Elsevier Inc. All rights reserved.
doi:10.1016/j.jcp.2004.10.022

Nomenclature

$\tilde{\phi}$	velocity potential	k_x, k_y	Cartesian components of wave number vector
t	time	ω	wave absolute frequency
x, y	rectangular coordinate system	θ	wave angle
ξ, η	curvilinear coordinate system	h	water depth
$\mathbf{r}$	position vector	$\mathbf{g_i}$, $\mathbf{g^i}$	covariant and contravariant base vector, respectively
$\mathbf{U}$	current velocity vector	v^i, v_i	contravariant and covariant components of an arbitrary vector $\mathbf{v}$
U, V	contravariant components of velocity vector	g^{ij}, g_{ij}	contravariant and covariant metric, respectively
u, v	Cartesian components of velocity vector	J	Jacobian value of coordinate transformation
C	wave celerity	p	CC_g
C_g	wave group velocity	A	wave amplitude complex
σ	wave intrinsic frequency	g	gravitation
k, $\mathbf{k}$	wave number and wave number vector, respectively	ζ	wave surface displacement
k_i	covariant component of wave number vector		
k_1'	approximated value for covariant component k_1		

diffraction and has been widely used especially for engineering purpose. Recent developments of the parabolic model include consideration of wave–current interaction effects, various forms of non-linearity, dissipation, and wave breaking. Some common limitations for model applications have been known as that the propagation direction of all major components of the wave field must be confined to some narrow band of directions centered on a prechosen principal propagation direction. A primary progress to relax the limitations has been made using higher-order approximations ([8]), which shows an obvious extension of validity range of the model equations. An alternative approach to relaxing the model restriction is to use curvilinear parabolic approximation in which curvilinear coordinate lines are chosen approximately along the predominant wave propagation directions. Several efforts to develop curvilinear parabolic models have been made by many authors. The early developments of the curvilinear models concentrated on solving irregular lateral boundary problems, particularly for idealized situations involving simple boundary configurations [11,15]. Tsay et al. [18] reported boundary-fitted curvilinear model in which lowest-order approximations have been made for several geometries. Kirby et al. [12] presented a curvilinear parabolic model that includes both the low-order approximation and the higher-order approximation and focused on conformal mapping though generalized curvilinear equations were given in their paper. In all the existing curvilinear parabolic models, wave–current interaction is not taken into account. Those curvilinear parabolic equations were derived from the elliptic equations of either the velocity potential or the free surface displacement, which are essentially equations of scalar variables. Therefore, the direct coordinate transformation which based on the differential relation between two coordinates can be simply applied. Although the equation of wave number vector, $\mathbf{k}$, may be used, for example, in the case of Tsay et al. [18], Cartesian components, (k_x, k_y) were usually kept in the equation, which made the final equation complex. For the more general vector equation which includes wave–current interaction terms such as the wave–current equation given by Booij [1] or Kirby [8], the direct transformation may not be an appropriate method for the purpose of simplicity of the model equation.

In the present paper, we start with the vector form of the wave–current equation given by Kirby [8], which takes into account the current effect on waves, wave dissipation caused by bottom friction or wave breaking and non-linear dispersion. Covariant components of the wave number vector (**k**) and contravariant components of the current velocity vector (**U**) are adopted for the parabolic approximation in the derivation of the curvilinear equation. The combination of the covariant **k** and contravariant **U** enable the derivation to follow closely the higher-order approximation in Cartesian coordinates in Kirby [8]. We expect that most terms in the resulting curvilinear equation can be found their counterparts in the Cartesian equation in Kirby [8] so that the curvilinear equation can be implemented easily following the model structure and numerical schemes used in the existing computational code REF/DIF-1 [13].

In the following section, the curvilinear parabolic approximation is presented in a generalized curvilinear coordinate system. Numerical schemes, boundary conditions and wave angle calculation based on curvilinear coordinates are given in Section 3. In Section 4, we show several examples of using the curvilinear parabolic model and discuss effects from the extra terms caused by grid stretching and non-orthogonality in the examples. Wave–current interaction is presented in one of the examples to demonstrate the accuracy and capability of the curvilinear model in predicting wave transformation in complex environments.

2. Derivation

We start with Kirby's [8] time-dependent wave–current equation which includes lowest-order amplitude dispersion for a Stokes wave and dissipation caused by bottom friction or wave breaking. The equation for the value of the velocity potential $\tilde{\phi}$ at the mean water level can be written as following, after neglecting the wave-induced long wave motion:

$$\frac{\mathrm{D}^2\tilde{\phi}}{\mathrm{D}t^2} + (\nabla_h \cdot \mathbf{U})\frac{\mathrm{D}\tilde{\phi}}{\mathrm{D}t} - \nabla_h \cdot (CC_g\nabla_h\tilde{\phi}) + (\sigma^2 - k^2CC_g)\nabla\tilde{\phi} + \sigma^2k^2D|A|^2\tilde{\phi} - \mathrm{i}\sigma w\tilde{\phi} = 0, \tag{1}$$

where **U** represents the current velocity vector. The operator D/Dt is given by

$$\frac{\mathrm{D}}{\mathrm{D}t} \equiv \frac{\partial}{\partial t} + \mathbf{U}\cdot\nabla_h, \tag{2}$$

where σ and **k** represent the wave intrinsic frequency and the wave number vector, respectively, and the dispersion relation can be determined according to

$$\sigma = \omega - \mathbf{k}\cdot\mathbf{U} = (gk\tanh kh)^{1/2}, \tag{3}$$

in which ω is the absolute frequency. In (1), D is the non-linear dispersion term according to Stokes waves and can be written as

$$D = \frac{\cosh 4kh + 8 - 2\tanh^2 kh}{8\sinh^4 kh}. \tag{4}$$

The final term in (1) is a dissipation term which may be used to model frictional dissipation [3,14] or wave breaking [10].

To ease the derivation of the curvilinear parabolic approximation, we follow Kirby's [8] derivation made in rectangular Cartesian coordinates. It is found that the initial parabolic approximations of vector operations in the wave–current equation are the key points to derive the curvilinear parabolic type equation that can keep the same form and the same approximation order as Kirby's [8] final equation.

In Kirby's [8] derivation, the dispersion relation (3) was approximated by

$$\sigma = \omega - |\mathbf{k}|u, \tag{5}$$

which is a reasonable approximation considering waves propagate dominantly in the x-direction. In the construction of the amplitude form of the parabolic equation in Kirby's [8], a progressive wave was described in the form

$$\tilde{\phi} \equiv -\frac{\mathrm{i}g}{2}\left(\frac{A}{\sigma}\right)\mathrm{e}^{\mathrm{i}\left(\int \bar{k}\ \mathrm{d}x-\omega t\right)} + \text{c.c.}, \tag{6}$$

in which wave transformation in the x-direction is dominant. The representative wavenumber $\bar{k}$ is obtained by an average over the transverse y-coordinate

$$\bar{k} = \frac{1}{y_2 - y_1}\int_{y_1}^{y_2} k(x,y)\ \mathrm{d}y. \tag{7}$$

To make curvilinear parabolic approximations of the wave–current equation, a coordinate transformation should be carried out prior to development of any approximation [11]. With Cartesian components of **U** and **k** retained in the derivation, the direct coordinate transformation method would result in a complicated form of the final equation because the dispersion relation (3)

$$\sigma = \omega - (k_x u + k_y v) \tag{8}$$

cannot be approximated to a simple form as in Kirby [8], and (6) will be extended to

$$\tilde{\phi} \equiv -\frac{\mathrm{i}g}{2}\left(\frac{A}{\sigma}\right)\mathrm{e}^{\mathrm{i}\left[\int (k_x x_\xi + k_y y_\xi)\ \mathrm{d}\xi + (k_x x_\eta + k_y y_\eta)\ \mathrm{d}\eta - \omega t\right]} + \text{c.c.} \tag{9}$$

in curvilinear coordinates. Both (8) and (9) include k_x and k_y neither of which can be used alone to represent the dominant component in a wave propagation direction.

In the following, the contravariant–covariant tensor method will be used for curvilinear parabolic approximations. It will be found that the combination of the covariant wavenumber **k** and contravariant velocity **U** reduce the vector operations to the same forms as in the Cartesian approximations, allowing the derivation to follow closely the procedure in Kirby [8].

In generalized horizontal 2-D coordinates, an arbitrary vector **v** can be expressed in a general form based on covariant base vectors ($\mathbf{g_1}$, $\mathbf{g_2}$) or the reciprocal contravariant base vectors ($\mathbf{g^1}$, $\mathbf{g^2}$)

$$\mathbf{v} = v^i \mathbf{g_i} = v_i \mathbf{g^i} \quad (i = 1, 2, \text{hereafter}), \tag{10}$$

where v^i and v_i represent contravariant component and covariant component, respectively, and $\mathbf{g^i}$ and $\mathbf{g_i}$ satisfy

$$\mathbf{g^i} \cdot \mathbf{g_j} = \delta^i_j, \tag{11}$$

in which δ^i_j is the Kronecker delta function.

The relation between covariant and contravariant components can be expressed as

$$v^i = g^{ik} v_k \tag{12}$$

and

$$v_i = g_{ik} v^k, \tag{13}$$

where g_{ik} and g^{ik} represent the covariant metric and contravariant metric, respectively. The Jacobian value J for coordinate transformation can be written in terms of g_{ij} by

$$J^2 = \begin{vmatrix} g_{11} & g_{12} \\ g_{21} & g_{22} \end{vmatrix}. \tag{14}$$

For a given curvilinear coordinate system expressed by ($\xi(x,y)$, $\eta(x,y)$), the metric tensor and Jacobian are given by:

$$\begin{aligned} g_{11} &= x_\xi^2 + y_\xi^2, \\ g_{12} &= g_{21} = x_\xi x_\eta + y_\xi y_\eta, \\ g_{22} &= x_\eta^2 + y_\eta^2, \end{aligned} \tag{15}$$

$$J = x_\xi y_\eta - x_\eta y_\xi \tag{16}$$

and

$$\begin{aligned} g^{11} &= g_{22}/J^2, \\ g^{12} &= g^{21} = -g_{12}/J^2, \\ g^{22} &= g_{11}/J^2. \end{aligned} \tag{17}$$

To facilitate the derivation in generalized coordinates, we use both the covariant and contravariant components in the expressions of vector variables. The contravariant components are used for position vector $\mathbf{r}$ and current velocity vector $\mathbf{U}$ as

$$\delta\mathbf{r} = \delta r^i \mathbf{g_i} = \delta\xi \mathbf{g_1} + \delta\eta \mathbf{g_2}, \tag{18}$$

$$\mathbf{U} = u^i \mathbf{g_i} = U\mathbf{g_1} + V\mathbf{g_2} \tag{19}$$

and covariant components are used for wave number vector $\mathbf{k}$ as

$$\mathbf{k} = k_i \mathbf{g^i} = k_1 \mathbf{g^1} + k_2 \mathbf{g^2}. \tag{20}$$

Using the contravariant components of $\mathbf{U}$ and $\mathbf{r}$, the operator D/Dt can be simply written as

$$\frac{\mathrm{D}}{\mathrm{D}t} = \frac{\partial}{\partial t} + u^i \frac{\partial}{\partial r^i} = \frac{\partial}{\partial t} + U\frac{\partial}{\partial \xi} + V\frac{\partial}{\partial \eta}. \tag{21}$$

Following the assumption made in the parabolic equation method in Cartesian coordinates, we assume that waves are oriented in the $+\xi$ direction in the general curvilinear coordinates. The dispersion relation may be written as

$$\sigma = \omega - k_i u^i = \omega - (k_1 U + k_2 V). \tag{22}$$

The similar approximation for the dispersion relation can be made following Kirby [8]. Noticing that the magnitude of $\mathbf{k}$ can be expressed by the covariant components (k_1, k_2) as following:

$$|\mathbf{k}| = k = \sqrt{g^{11}k_1^2 + 2g^{12}k_1k_2 + g^{22}k_2^2}, \tag{23}$$

we now set

$$k_1' = k/\sqrt{g^{11}}, \tag{24}$$

where k_1' is a reasonable approximate value for the covariant component k_1. The dispersion relation is thus approximated by

$$\sigma = \omega - k_1' U, \tag{25}$$

consistent with the Cartesian approximation in Kirby [8]. Eq. (24) will be used in the derivation of the model equation and the superscript "′" will be dropped hereafter.

After substituting for the harmonic time dependence, Eq. (1) may then be written as

$$[(g^{11}p - U^2)\tilde{\phi}_\xi]_\xi + k_1^2(pg^{11} - U^2)\tilde{\phi} + M\tilde{\phi} + S\tilde{\phi} = 0, \tag{26}$$

where $p = CC_g$, $M\tilde{\phi}$ is given by

$$\begin{aligned} M\tilde{\phi} = {} & [2\omega k_1 U + \mathrm{i}\omega\frac{1}{J}[(JU)_\xi + (JV)_\eta] - \sigma^2 k_1^2 g^{11} D|A|^2 + \mathrm{i}\sigma w]\tilde{\phi} - (UV\tilde{\phi}_\eta)_\xi - (UV\tilde{\phi}_\xi)_\eta \\ & + [(g^{22}p - V^2)\tilde{\phi}_\eta]_\eta + 2\mathrm{i}\omega(U\tilde{\phi}_\xi + V\tilde{\phi}_\eta) \end{aligned} \tag{27}$$

and $S\tilde{\phi}$ contains extra terms caused by grid stretching and non-orthogonality and is given by

$$S\tilde{\phi} = (g^{21}p\tilde{\phi}_\eta)_\xi + \frac{J_\xi}{J}p\left(g^{11}\tilde{\phi}_\xi + g^{21}\tilde{\phi}_\eta\right) + (g^{12}p\tilde{\phi}_\xi)_\eta + \frac{J_\eta}{J}p\left(g^{12}\tilde{\phi}_\xi + g^{22}\tilde{\phi}_\eta\right). \tag{28}$$

The above derivation of the elliptic type equation has used (21), (25) and the following divergence formula in generalized curvilinear coordinates:

$$\mathrm{div}(\mathbf{v}) = \frac{1}{J}\frac{\partial Jv^i}{\partial x^i}. \tag{29}$$

Compared to the elliptic type equation in Cartesian coordinates, (26) and (27) are very similar to Eqs. (43) and (44) in Kirby [8] except the covariant component k_1 and contravariant components (U, V) are used in the present equations. In addition, the metric tensor g^{ij} show up in some terms where p appears.

Using a splitting method following Booij [1] (Appendix A), the parabolic equation may be written as

$$\begin{aligned} & \sigma(\sqrt{g^{11}}C_g + U)\tilde{\phi}_\xi + \frac{1}{2}\left[\sigma(\sqrt{g^{11}}C_g + U)\right]_\xi\tilde{\phi} - \mathrm{i}k_1\sigma(\sqrt{g^{11}}C_g + U)\tilde{\phi} + \frac{\mathrm{i}}{2}\sigma^2 k_1^2 g^{11} D|A|^2\tilde{\phi} + \sigma\frac{w}{2}\tilde{\phi} \\ & - \left[\omega U\tilde{\phi}_\xi + \frac{1}{2}(\omega U)_\xi\tilde{\phi} - \mathrm{i}k\omega U\tilde{\phi}\right] - \mathrm{i}\frac{3}{4}M'\tilde{\phi} + \frac{1}{4k_1}(M'\tilde{\phi})_\xi - \frac{1}{4}\beta(M')\tilde{\phi} - \frac{\mathrm{i}}{2}S\tilde{\phi} = 0, \end{aligned} \tag{30}$$

where $M'\tilde{\phi}$ is derived from $M\tilde{\phi}$ by neglecting the non-linear and friction terms and where

$$\beta = \frac{k_{1\xi}}{k_1^2} + \frac{[k_1(g^{11}p - U^2)]_\xi}{2k_1^2(g^{11}p - U^2)}. \tag{31}$$

To construct the amplitude form of the parabolic equation, we may assume that the wave consists of a progressive wave which has $+\xi$ as the preferred propagation direction. $\tilde{\phi}$ may be written in the form

$$\tilde{\phi} \equiv -\frac{\mathrm{i}g}{2}\left(\frac{A}{\sigma}\right)\mathrm{e}^{\mathrm{i}\left(\int \bar{k_1}\,\mathrm{d}\xi - \omega t\right)} + \mathrm{c.c.}, \tag{32}$$

where $\bar{k_1}$ is obtained by an average of k_1 over the transverse η-coordinate

$$\bar{k_1} = \frac{1}{\eta_2 - \eta_1}\int_{\eta_1}^{\eta_2} k_1(\xi,\eta)\,\mathrm{d}\eta. \tag{33}$$

It should be noted that the definition of $\bar{k_1}$ is different from the definition of the reference phase function based on $k_0(\xi) \times J_0(\xi)$ in Kirby et al. [12], which is only valid for conformal coordinate transformations. After dropping some terms according to the same criteria as in Kirby [8], the final form of the equation may be written as

$$(\sqrt{g^{11}}Cg+U)A_\xi+VA_\eta+\mathrm{i}(\bar{k}_1-k_1)(\sqrt{g^{11}}C_\mathrm{g}+U)A+\frac{\sigma}{2}\left[\left(\frac{\sqrt{g^{11}}C_\mathrm{g}+U}{\sigma}\right)_\xi+\left(\frac{V}{\sigma}\right)_\eta\right]A$$
$$-\frac{\mathrm{i}}{2}\left[(g^{22}p-V^2)\left(\frac{A}{\sigma}\right)_\eta\right]_\eta+\frac{\mathrm{i}}{2}\left\{\left[UV\left(\frac{A}{\sigma}\right)_\eta\right]_\xi+\left[UV\left(\frac{A}{\sigma}\right)_\xi\right]_\eta\right\}+\frac{\mathrm{i}\sigma}{2}k_1^2g^{11}D|A|^2A+\frac{w}{2}A$$
$$+\frac{1}{4k_1}\left\{\left[(g^{22}p-V^2)\left(\frac{A}{\sigma}\right)_\eta\right]_{\eta\xi}+2\mathrm{i}\left[\sigma V\left(\frac{A}{\sigma}\right)_\eta\right]_\xi\right\}$$
$$+\frac{\beta}{4}\left\{2\mathrm{i}\omega U\left(\frac{A}{\sigma}\right)_\xi+2\mathrm{i}\sigma V\left(\frac{A}{\sigma}\right)_\eta-2UV\left(\frac{A}{\sigma}\right)_{\xi\eta}+\left[(g^{22}p-V^2)\left(\frac{A}{\sigma}\right)_\eta\right]_\eta\right\}$$
$$+\frac{\mathrm{i}}{4k_1}\left[(\omega V)_\eta+3(\omega U)_\xi\right]\left(\frac{A}{\sigma}\right)_\xi+S'=0, \tag{34}$$

where S' represents terms related to grid stretching and non-orthogonality and may be written as

$$S'=-\frac{\mathrm{i}}{2}g^{12}\left[p\left(\frac{A}{\sigma}\right)_\eta\right]_\xi-\frac{\mathrm{i}}{2}g^{12}\left[p\left(\frac{A}{\sigma}\right)_\xi\right]_\eta-\frac{\mathrm{i}}{2}\frac{p}{J}\left(\frac{A}{\sigma}\right)_\xi(J_\xi g^{11}+J_\eta g^{12})-\frac{\mathrm{i}}{2}\frac{p}{J}\left(\frac{A}{\sigma}\right)_\eta(J_\xi g^{12}+J_\eta g^{22})$$
$$+\bar{k}_1pg^{12}\left(\frac{A}{\sigma}\right)_\eta+\frac{\bar{k}_1}{2}g^{12}\left(\frac{A}{\sigma}\right)p_\eta+\frac{\bar{k}_1}{2}\frac{p}{J}\left(\frac{A}{\sigma}\right)(J_\xi g^{11}+J_\eta g^{12}). \tag{35}$$

Eq. (35) contains all the terms induced by grid stretching and non-orthogonality. In fact, our test cases show that the first three terms in (35) are very small terms and can be neglected in all the cases shown in Section 4. A scaling analysis for those terms is not given in this study because coordinate transformation parameters, such as the Jacobian and metric tensors, are case-dependent.

3. Model implementation

3.1. Numerical schemes

Comparing the model equation (34) to the Cartesian equation [8] shown in Appendix B, we can easily find that, except S' term, each term in (34) has its counterpart in the Cartesian equation (B.1). Therefore, the numerical schemes and other existing implementation techniques used in REF/DIF-1 [13] can be directly adopted in the present model. The present model implementation includes energy dissipation, subgrid technique and high-frequency damping. The non-linearity evaluated by the lowest-order Stokes formulation of Kirby and Dalrymple [7] is also taken into account in the model.

Eq. (34) is discretized using the Crank–Nicolson method, matching forward in ξ. Iterations for the nonlinear terms are performed using a repeated implicit calculation. The additional term S' is also discretized using the Crank–Nicolson scheme. The metric tensor and Jacobian values are calculated at computational grid points and interpolated into subgrid if needed. Grid spacing in the image domain is uniform, i.e., $\Delta\xi=\Delta\eta=1$.

3.2. Initial and lateral boundary conditions

The initial condition is specified at the furthest seaward grid row. For given wave amplitude a, wave number k and wave angle θ (based on x-direction in Cartesian coordinates), the input initial condition can be written as

$$A = a\mathrm{e}^{\mathrm{i}\int k_2\,\mathrm{d}\eta} = a\mathrm{e}^{\mathrm{i}\int (x_\eta k\cos\theta + y_\eta k\sin\theta)\,\mathrm{d}\eta}. \tag{36}$$

The reflective boundary condition is implemented for the lateral boundaries in the present model. The reflective boundary condition may be written as

$$\nabla\tilde{\phi}\cdot\mathbf{g^2} = 0, \tag{37}$$

where $\mathbf{g^2}$ is the contravariant base vector defined in (10). Applying the covariant components of $\nabla\tilde{\phi}$ in (37) directly yields the full boundary condition

$$g^{12}\left[\left(\frac{A}{\sigma}\right)_\xi + \mathrm{i}\bar{k_1}\frac{A}{\sigma}\right] + g^{22}\left(\frac{A}{\sigma}\right)_\eta = 0. \tag{38}$$

For the case without considering of the Doppler effect on waves, (38) can be simplified to

$$g^{12}(A_\xi + \mathrm{i}\bar{k_1}A) + g^{22}A_\eta = 0. \tag{39}$$

The boundary condition may be incorporated in the numerical scheme without difficulty and is thus not further approximated.

3.3. Wave angle calculation

The convenient way to demonstrate wave direction in generalized curvilinear coordinates is to use a linear axis, e.g. x-axis in a rectangular Cartesian frame, as an invariant direction reference. In the present model, zero angle is set to $+x$-direction, as in the Cartesian model. Because covariant/contravariant tensors are used in the model equation, the formulation for wave angle calculations is different from that in the Cartesian model. In the Cartesian model, the wave surface displacement can be written by

$$\zeta = A\mathrm{e}^{\mathrm{i}\int \bar{k}\,\mathrm{d}x} = |A|\mathrm{e}^{\mathrm{i}\int(\delta k_x+\bar{k})\,\mathrm{d}x+\mathrm{i}\int k_y\,\mathrm{d}y}, \tag{40}$$

which implies

$$\delta k_x + \bar{k} = k_x \tag{41}$$

and δk_x can evaluated by

$$\delta k_x = \Im\left[\frac{\partial}{\partial x}(\ln A)\right]. \tag{42}$$

Wave angle can be calculated by

$$\theta = \arctan\left(\frac{k_y}{\delta k_x + \bar{k}}\right). \tag{43}$$

Similarly, in the curvilinear coordinates, the wave surface displacement can be written by

$$\zeta = |A|\mathrm{e}^{\mathrm{i}\int(\delta k_1+\bar{k_1})\,\mathrm{d}\xi+\mathrm{i}\int k_2\,\mathrm{d}\eta}, \tag{44}$$

where δk_1 can be calculated by

$$\delta k_1 = \mathrm{image}\left[\frac{\partial}{\partial\xi}(\ln A)\right]. \tag{45}$$

According to the chain rule, (44) may be written as

$$\zeta = |A|\mathrm{e}^{\mathrm{i}\int[(\delta k_1+\bar{k_1})\xi_x+k_2\eta_x]\,\mathrm{d}x+\mathrm{i}\int[(\delta k_1+\bar{k_1})\xi_y+k_2\eta_y]\,\mathrm{d}y}. \tag{46}$$

The wave angle formula can be written as

$$\theta = \arctan\left[\frac{(\delta k_1 + \bar{k}_1)\xi_y + k_2\eta_y}{(\delta k_1 + \bar{k}_1)\xi_x + k_2\eta_x}\right], \tag{47}$$

where ξ_x, ξ_y, η_x and η_y are calculated by

$$\xi_x = y_\eta/J, \quad \xi_y = -x_\eta/J, \quad \eta_x = -y_\xi/J, \quad \eta_y = x_\xi/J. \tag{48}$$

3.4. Curvilinear grid generation and metric tensor calculation

In contrast to model equations derived based on some specific algebraic coordinate transformation, e.g. Liu and Boissevain [15] or Kirby [11], the present model equation does not explicitly involve any grid generation methods or equations. However, grids from different grid generation methods may cause some differences in the wave model results because the parabolic approximation is made along curvilinear grid lines and the model equation is discretized in finite difference schemes.

A curvilinear grid can be generated using either algebraic formulas or grid generation softwares. The generated curvilinear grid lines should approximately follow the directions of wave propagation to keep the wave calculations in the validity range of the parabolic model equation (70° wave angles with respect to the direction of coordinate lines as suggested by [9]). To incorporate the grid generation results into the wave model, $x(\xi,\eta)$, $y(\xi,\eta)$ obtained from the solution of the grid generation formulas/equations are used to calculate the curvilinear coordinate-related parameters, i.e., the Jacobian J and metric tensors g^{11}, g^{22} and g^{12} required by the curvilinear model equation (34). A second-order central difference scheme is used to calculate the Jacobian and metric tensors according to (15)–(17).

In two test cases shown in the next section, we use the grid generation method based on Brackbill and Saltzman's [2] equations. This grid generation is carried out by numerically solving a set of Euler equations optimizing simultaneously grid smoothness, orthogonality, and weighted grid density. Interested readers can download the grid generation software at http://chinacat.coastal.udel.edu/kirby/programs/index.html.

4. Model applications

We now carry out several model applications involving curvilinear coordinates. In the first application, waves propagate in either the radial direction or tangential direction in a circular channel and an orthogonal curvilinear grid is used. The test case is used to examine the curvilinear terms caused by grid stretching. To test the terms resulting from non-orthogonality, we generate a non-orthogonal grid in the second application, Isobe's [6] laboratory experiment, in which waves propagate into a harbor formed by two diverging breakwaters. In the last application, we simulate [5] experiment in which waves and wave-induced currents were measured on a curved beach. A generalized curvilinear grid system is employed to follow principle wave directions and fit breakwater and beach boundaries. The purpose of the simulation is also to test the model performance in predicting wave–current interaction in a complicated domain.

4.1. Waves in circular channel

In the present model equation, grid stretching can be represented by J_ξ and J_η in (35). To demonstrate the effect of grid stretching on wave calculations, we show a case with an orthogonal computational grid and varying Jacobian values.

The computational domain is a round tank with constant water depth. The first test is that cylindrical waves are generated at the inner cylinder and then propagate normally to the outer boundary. The curvilinear coordinates for this case can be defined by

$$\begin{aligned} x &= \left[r_0 + \frac{(r_1 - r_0)}{l_1}\xi\right]\cos\left(\frac{2\pi}{l_2}\eta\right), \\ y &= \left[r_0 + \frac{(r_1 - r_0)}{l_1}\xi\right]\sin\left(\frac{2\pi}{l_2}\eta\right), \end{aligned} \tag{49}$$

where r_0 and r_1 are the radii of inner boundary and outer boundary, respectively. $\xi = (0 \sim l_1)$ and $\eta = (0 \sim l_2)$.

Using (15)–(17) results in

$$J = \frac{2\pi(r_1 - r_0)}{l_1 l_2}\left(r_0 + \frac{r_1 - r_0}{l_1}\xi\right), \tag{50}$$

$$J_\xi = \frac{2\pi(r_1 - r_0)^2}{l_1^2 l_2}, \quad J_\eta = 0, \tag{51}$$

$$g^{11} = \frac{l_1^2}{(r_1 - r_0)^2}, \quad g^{12} = 0, \quad g^{22} = \frac{1}{4\pi^2}\frac{l_2^2}{(r_0 + \frac{r_1 - r_0}{l_1}\xi)^2}. \tag{52}$$

Thus S' can be simplified to

$$S' = \frac{\bar{k_1}}{2}\frac{p}{J}J_\xi g^{11}\left(\frac{A}{\sigma}\right). \tag{53}$$

It can be seen from (50) that the Jacobian increases linearly from the inner boundary to outer boundary in this case. Because $\sqrt{g^{11}}$ is constant in the whole domain, the stretching term in (53) plays a key role in wave calculations.

Noticing the constant $\sqrt{g^{11}}$ and $\partial/\partial\eta = 0$, the model equations (34) and (35) can be simplified to

$$\sqrt{g^{11}}C_g A_\xi + \frac{\bar{k_1}}{2}\frac{p}{J}\left(\frac{A}{\sigma}\right)J_\xi g^{11} = 0. \tag{54}$$

Utilizing $\bar{k_1} = \bar{k}/\sqrt{g^{11}}$ and $pk/C_g\sigma = 1$ (54) can be further simplified to

$$A_\xi = -\frac{1}{2}\frac{J_\xi}{J}A. \tag{55}$$

Applying $A^* \times (55) + A \times (55)^*$ yields

$$\frac{\partial J|A|^2}{\partial\xi} = 0. \tag{56}$$

Using the boundary conditions

$$A = A_0; \quad J = J_0 \text{ at } \xi = 0 \tag{57}$$

results in

$$|A|^2 = |A_0|^2\frac{J_0}{J} \tag{58}$$

or

$$|A|^2 = |A_0|^2 \frac{r_0}{r}, \tag{59}$$

which is the wave energy conservation.

As an alternative test on the stretching terms, specifically the J_η-related term, the study on wave propagation along the circular channel is carried out. Dalrymple et al. [4] used spectral methods with coordinate-transformed equations to analytically study linear wave propagation in a circular channel. This case was also investigated numerically using a parabolic approximation model in conformal coordinate systems by Kirby et al. [12] who found that the higher-order approximation can improve calculations significantly in comparison to the analytical solutions.

Because the parabolic approximation is made in $+\xi$-direction in the model derivation, the expression of the curvilinear coordinates for this case would not be the same as (49). The curvilinear coordinates can be defined by

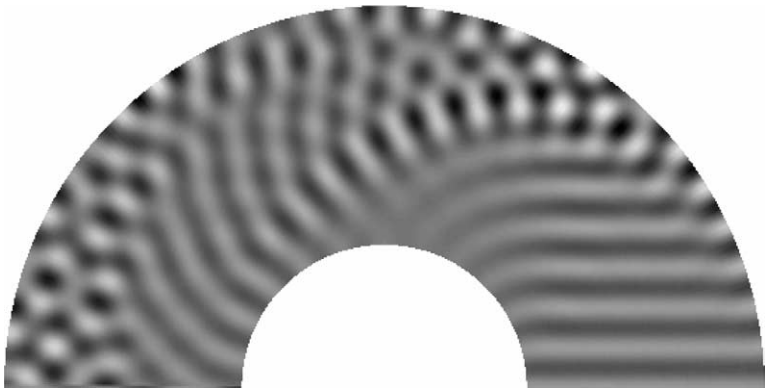

Fig. 1. Waves in the circular channel.

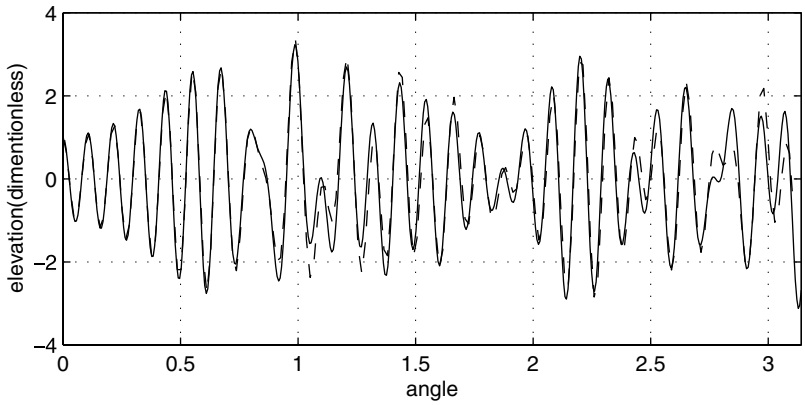

Fig. 2. Comparison of the surface variation along outer wall between the analytic solution (solid line) and numerical solution (dashed line).

$$x = \left[r_1 - \frac{(r_1 - r_0)}{l_1}\eta\right]\cos\left(\frac{2\pi}{l_2}\xi\right),$$
$$y = \left[r_1 - \frac{(r_1 - r_0)}{l_1}\eta\right]\sin\left(\frac{2\pi}{l_2}\xi\right). \tag{60}$$

Therefore, the Jacobian and its derivatives and metric tensor for this case are also changed to

$$J = \frac{2\pi(r_1 - r_0)}{l_1 l_2}\left(r_1 - \frac{r_1 - r_0}{l_1}\eta\right), \tag{61}$$

$$J_\eta = -\frac{2\pi(r_1 - r_0)^2}{l_1^2 l_2}, \quad J_\xi = 0, \tag{62}$$

$$g^{22} = \frac{l_1^2}{(r_1 - r_0)^2}, \quad g^{12} = 0, \quad g^{11} = \frac{1}{4\pi^2}\frac{l_2^2}{(r_1 - \frac{r_1 - r_0}{l_1}\eta)^2}. \tag{63}$$

The stretching term becomes to

$$S' = -\frac{\mathrm{i}}{2}\frac{p}{J}J_\eta g^{22}\left(\frac{A}{J}\right)_\eta. \tag{64}$$

Eq. (64) implies that the stretching term has an effect on wave diffraction.

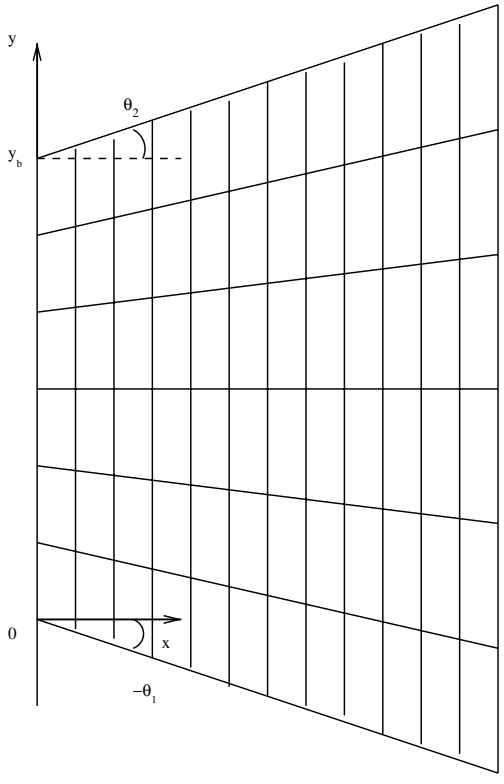

Fig. 3. Non-orthogonal grid for waves between angled boundaries.

Following the case study in Dalrymple et al. [4] and Kirby et al. [12], the circular channel lies between two radii $r_0 = 75$ m and $r_1 = 200$ m, and covers a 180° arc. As a particular choice of geometry and wave conditions, we set that water depth is 4 m and wave period is 4 s. The grid dimension is 201×126 ($l_1 = 125$ and $l_2 = 200$). Plane waves with a uniform amplitude across the channel are imposed at the entrance. Only linear waves are considered, since the exact solution does not have a non-linear counterpart.

Fig. 1 shows a plot of the instantaneous water surface calculated from the model. The figure illustrates the wave transformation phenomena described in Dalrymple et al. [4] and Kirby et al. [12] and also shows the capability of the curvilinear model in predicting wave reflections from the sidewall and diffractions around the inner wall. In Fig. 2, we show a comparison of the surface elevation variation along the outer wall. The parabolic model results show very good agreement with the exact solution with accurate phase and amplitude around the entire 180° sector. The present model results are very similar to the results from the conformal coordinate model with the large angle approximation Kirby et al. [12] since the same higher-order approximation is used in the present model equation. Considering that the present grid is not a conformal grid, the different treatments for $\bar{k}_1$ in the present model and $k_0(\xi)$ and $J_0(\xi)$ in Kirby et al. [12] may cause some small differences between two model results.

It should be mentioned that the rectangular Cartesian version of the parabolic wave model (e.g. [8]) would not be an appropriate model for this case since the tank circumferences can not be treated as the lateral boundaries of the Cartesian model. Waves are reflected from the boundaries around the channel and the wave angles with respect to the prechosen x-direction are too large. On the contrary, with the circular walls as its lateral boundaries, the curvilinear model can take into account the wave reflections and

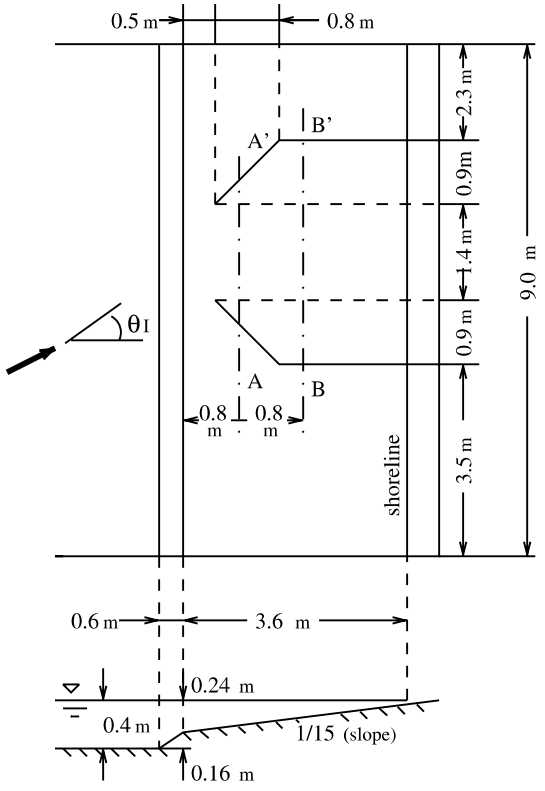

Fig. 4. Basin configuration for Isobe's experiments [6].

wave angles with respect to the circumferential coordinates would be in the validity range of the model equation according to the model evaluation based on the large angle approximation [9]. Therefore, the present model can make a good prediction of wave propagations in the circular channel.

4.2. Waves between diverging breakwaters

Wave propagation between two diverging breakwaters has been studied by several authors. Isobe [6] carried out a laboratory experiment to study waves propagating into a harbor formed by two diverging breakwaters. He then used a ray-front coordinate scheme [17] to numerically simulate the case. Liu and Boissevain [15] developed a non-orthogonal, rectilinear coordinate scheme for this case by applying a specific coordinate transformation to the a parabolic type equation and boundary conditions. Kirby [11] pointed out that a transformation of full governing equation prior to development of any approximation

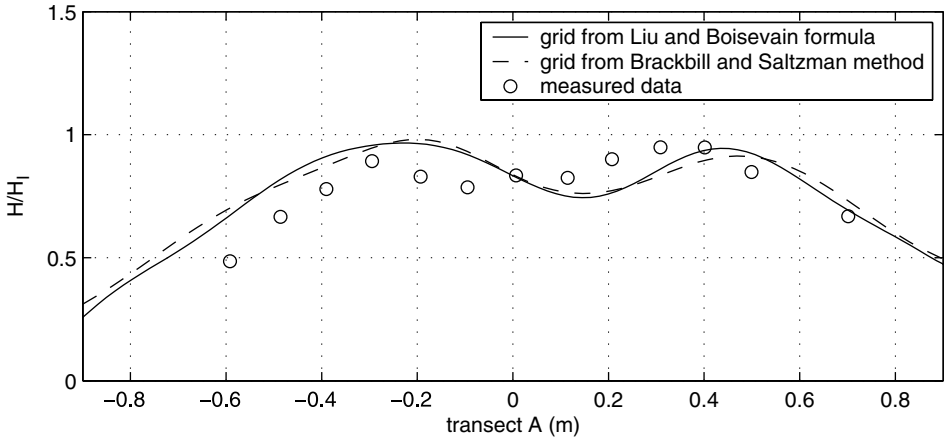

Fig. 5. Comparison of calculated and measured wave height distributions along transect A.

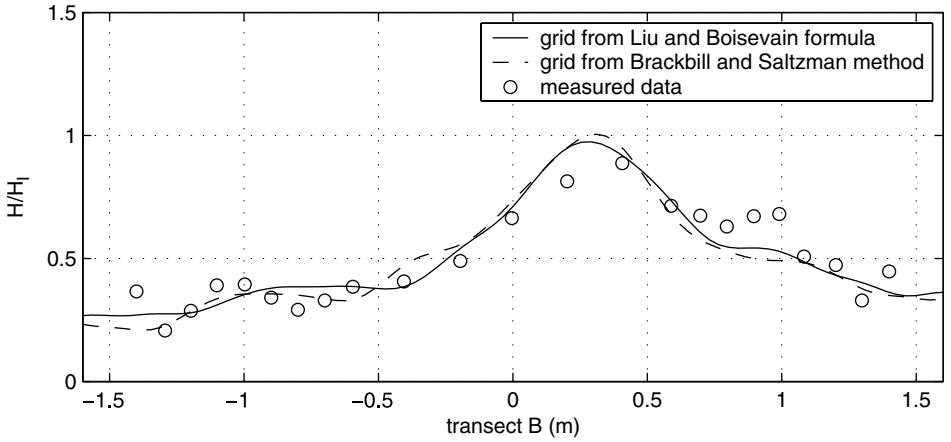

Fig. 6. Comparison of calculated and measured wave height distributions along transect B.

leads to a model whose results stand in closer agreement to laboratory data for this case. The importance of non-linear effects on wave calculations in the specific case was mentioned in Kirby [11].

The non-orthogonal coordinate transformation used by Liu and Boissevain [15] or Kirby [11] is a good example to test non-orthogonal terms for the present model. The grid system is shown in Fig. 3 and the coordinate transformation may be written as

$$\begin{cases} \xi = x, \\ \eta = \frac{y_b(y - x\tan\theta_1)}{(\tan\theta_2 - \tan\theta_1)x + y_b}. \end{cases} \tag{65}$$

Angles θ_1 and θ_2 are both defined to be positive in the right-handed sense in (x,y). The grid non-orthogonality is indicated by the value of g^{12} which can be calculated from (15) and (17) as

$$g^{12} = \frac{-y_b\tan\theta_1 - \eta(\tan\theta_2 - \tan\theta_1)}{(\tan\theta_2 - \tan\theta_1)\xi + y_b}. \tag{66}$$

It can be seen that g^{12} varies in both ξ and η directions.

The configuration for Isobe's [6] experiment is shown in Fig. 4. Isobe gave the incident wave conditions in the deep portion of the basin as incident direction $\theta_I = 18°$, wave height $H_I = 9.1$ cm, and wave period $T = 0.83$ s. These values were transformed to the harbor entrance using Snell's law, and then the present

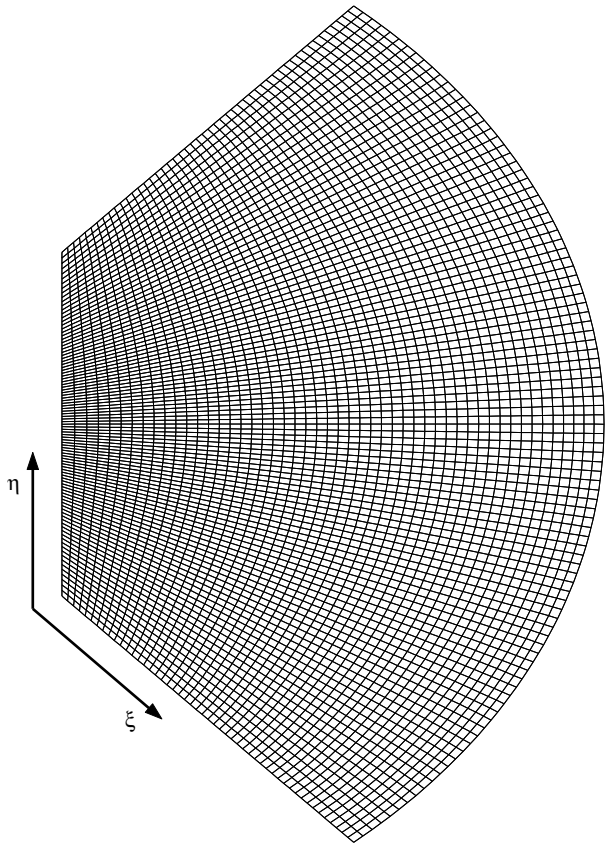

Fig. 7. Grid generated using Brackbill and Saltzman's [2] equations.

model is applied in order to compute wave heights at transect A − A′ and B − B′ indicated in Fig. 4. In the computations, $\xi = 51$ and $\eta = 51$. The non-linear term is included in the calculation.

In Fig. 5 and 6, the model results (solid lines) are compared to the measured data on transect A − A′ and B − B′, respectively. Results on transect A − A′ indicate that the present model basically captures the two wave height peaks caused by the wave diffraction as shown in the measurements. The results on transect B − B′ also show a good agreement to measurements. The results look very similar to Kirby's [11] results in his simulation with consideration of the non-linear effect. Although we expected some improvements on calculations of wave diffractions in this case since the high-order approximation is used in the present model, no significant enhancement of the model results is found. In addition, the full boundary condition was found to be critical in obtaining accurate results of this case.

To make a test on the model dependency on grid generation, we generate an alternative curvilinear grid using Brackbill and Saltzman's [2] grid generation method as shown in Fig. 7. The generated grid tends to be orthogonal compared to the analytical grid shown in Fig. 3. The wave modeling results based on the new grid are also shown in Fig. 5 and 6 in dashed lines. The new results are close to the previous results on both transect A − A′ and transect B − B′ though some discrepancies can be identified. The discrepancies are suspected to be caused by the non-orthogonality terms and lateral boundary conditions considering of the more orthogonal grid from Brackbill and Saltzman's equations.

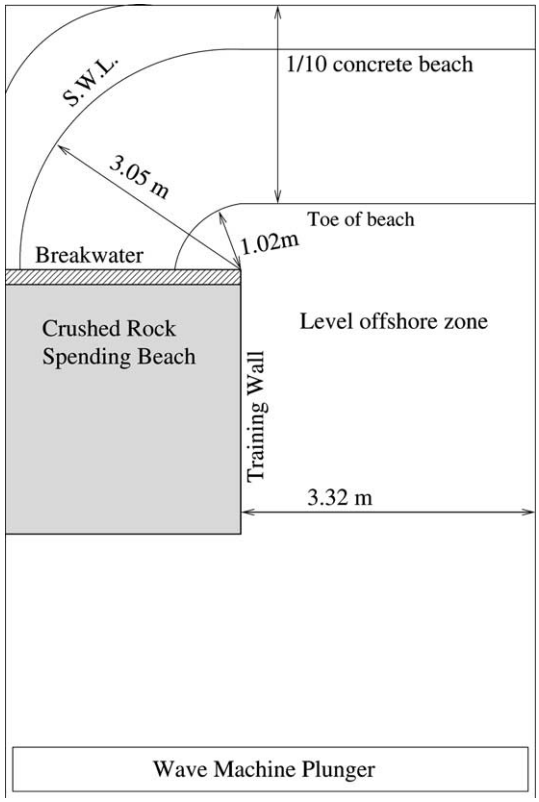

Fig. 8. Layout of Gourlay's experiment.

4.3. Waves passing breakwater and curved beach

Compared to the previous curvilinear parabolic approximation model, one versatility of the present model is incorporation of the current effect into the wave calculations. To illustrate the performance of the present model in predicting wave–current interaction, we now simulate Gourlay's [5] wave–current experiment in which waves pass a breakwater and break on a curved beach. The breaking waves generate longshore currents and affect wave propagations.

Fig. 8 shows the laboratory setup for Gourlay's experiment. A 1 on 10 concrete beach is parallel to the incoming wave crests in the exposed zone. In the shadow zone, the slope is also 1/10 towards the curved beach which has a constant radius centered on the breakwater tip. The wave basin was thus designed so that the shoreline was everywhere approximately parallel with the diffracted wave crests.

A curvilinear grid shown in Fig. 9 is generated using Brackbill and Saltzman's [2] grid generation equations. It can be seen that the grid approximately follow the principle wave directions and fit the curved shoreline boundary. The grid dimension $\xi \times \eta = 121 \times 193$. It can be seen from the figure that, at the tip of the breakwater, the curvilinear lines bend 90° in order to fit the breakwater boundary. The grid is smoothen around the tip to avoid a big grid distortion which may cause the discontinuity of the metric tensor.

A wave height of 9.1 cm with a wave period of 1.54 s is used in the present simulation as the incident wave condition, as in the laboratory experiment. We first run the model without the current effect. The wave surface calculated from the model is demonstrated in Fig. 10. The waves initially propagate in a

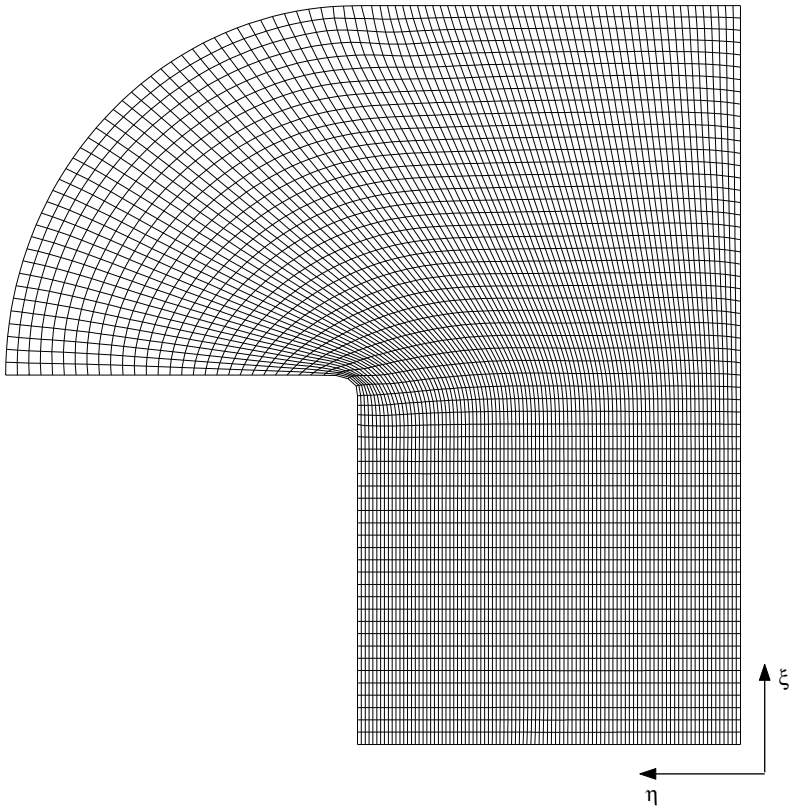

Fig. 9. Computational grid for simulation of Gourlay's experiment.

straight line along the channel, as reaching the tip of the breakwater, the waves start to diffract around the tip and run onto the curved beach. The diffracted wave crests are clear shown in the figure. Fig. 11 shows the wave height distribution calculated from the present model. The wave height contours show the wave diffractions in a radiate manner which is similar to the diffraction pattern in a typical case of normal wave incidence on a semi-infinite breakwater. The wave height contours also illustrate the wave height decay on the beach caused by wave breaking. To compare the results to the laboratory measurements, we plot the measured wave height contours according to Gourlay's measurements as shown in Fig. 12. The overall agreement of calculated wave height to the measurements is good. In particular, the calculated wave heights in the shadow region are between 2 and 4 cm, that match the measurement data. On the right-hand side of the breakwater tip, 10 cm contour in the numerical results is presented in the higher position compared to the measurements. In addition, the model without wave–current interaction does not predict the 10 cm contour as shown near the right side wall in Fig. 12.

We now consider the current effect on the wave propagation for the case. A model coupling is carried out between the present wave model and the curvilinear nearshore circulation model developed by Shi et al. [16]. The wave model provides the circulation model with radiation stresses, short-wave-induced volume flux and breaking wave energy dissipation. As a feedback, the current field calculated from the circulation model is inputed into the wave model and thus the wave–current interaction is taken into account. The currents calculated from the circulation model is illustrated by both the contours for the magnitude of the velocity and some streamlines indicating the direction of the flow in Fig. 13. The calculated current field agrees well with the measurements which is not presented here. Interested readers may refer to Gourlay [5] or Shi et al. [16] for details.

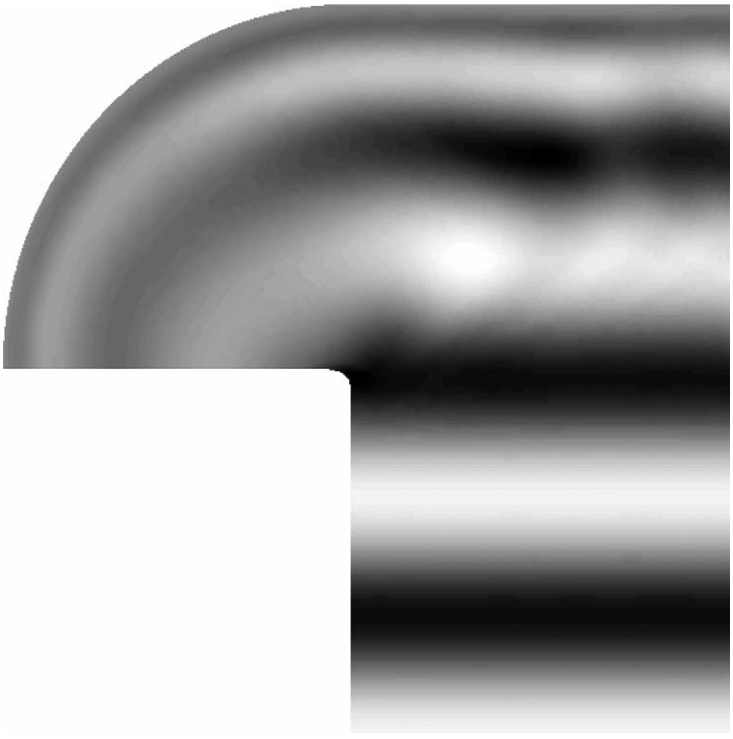

Fig. 10. Wave surface calculated by the present model without wave–current interaction.

With wave–current interaction, wave crests in both the explored region and the sheltered region are distorted by the currents as shown in Fig. 14. Fig. 15 shows the wave height distribution in the case of wave–current interaction. Compared to the previous results without wave–current interaction, the present results agree more closely to the measurements. Basically, the wave heights at the location where the curved beach starts tend to decrease because the current approximately flows in the wave direction. The wave heights near the right boundary tend to increase because the rip current flows against the waves. The 10 cm contour is predicted in the rip current region, that is consistent with the measurements.

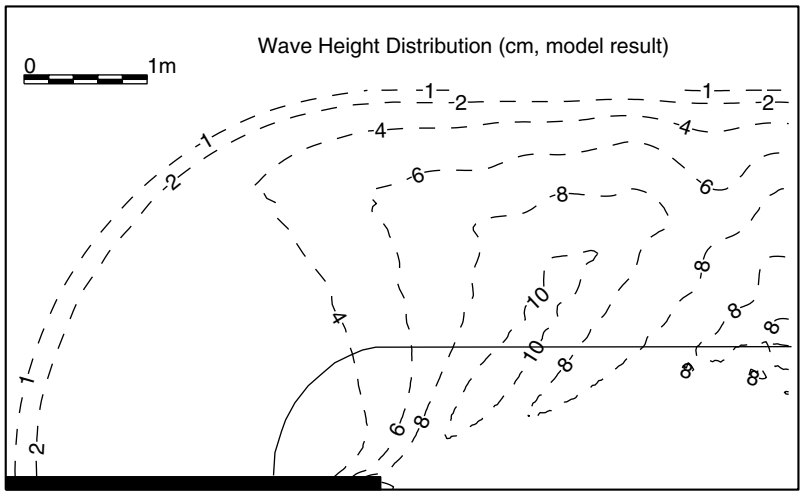

Fig. 11. Wave height calculated by the present model without wave–current interaction.

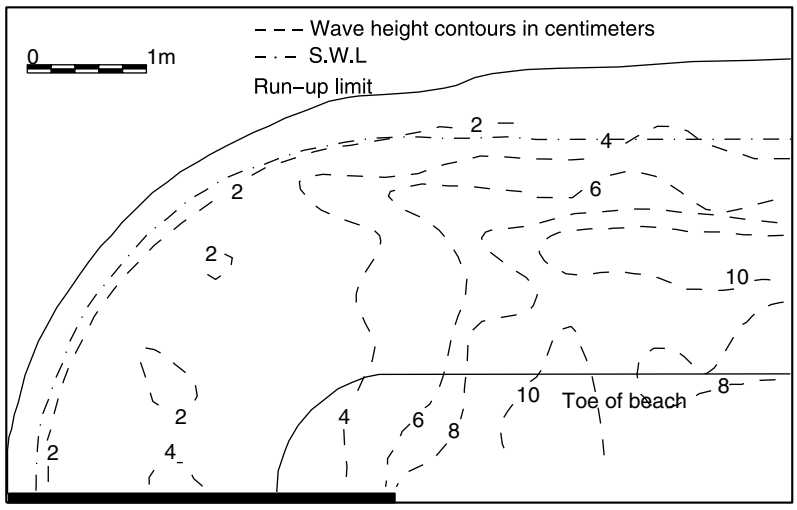

Fig. 12. Wave height contour measured in Gourlay's experiment.

The enhancement of the present model in predicting wave diffraction in the sheltered region can be presented by the comparison between the curvilinear model and the Cartesian model in Gourlay's case. To show the comparison, the Cartesian wave model REF/DIF-1 is employed in the model coupling

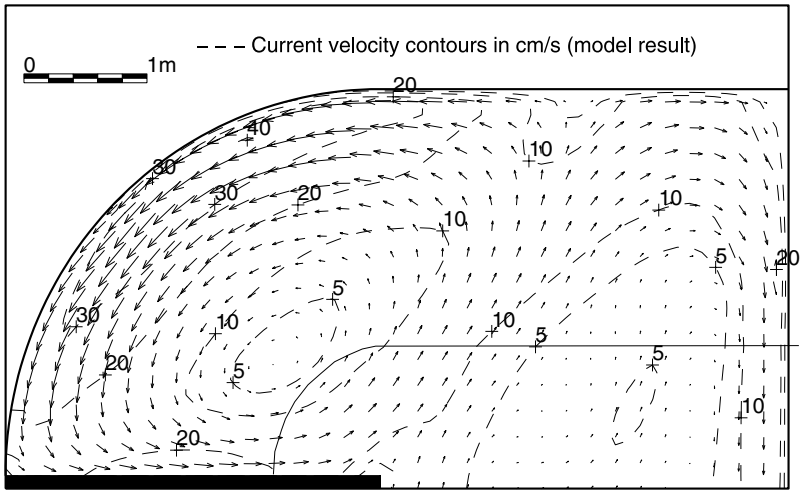

Fig. 13. Wave-induced current calculated by the nearshore circulation model.

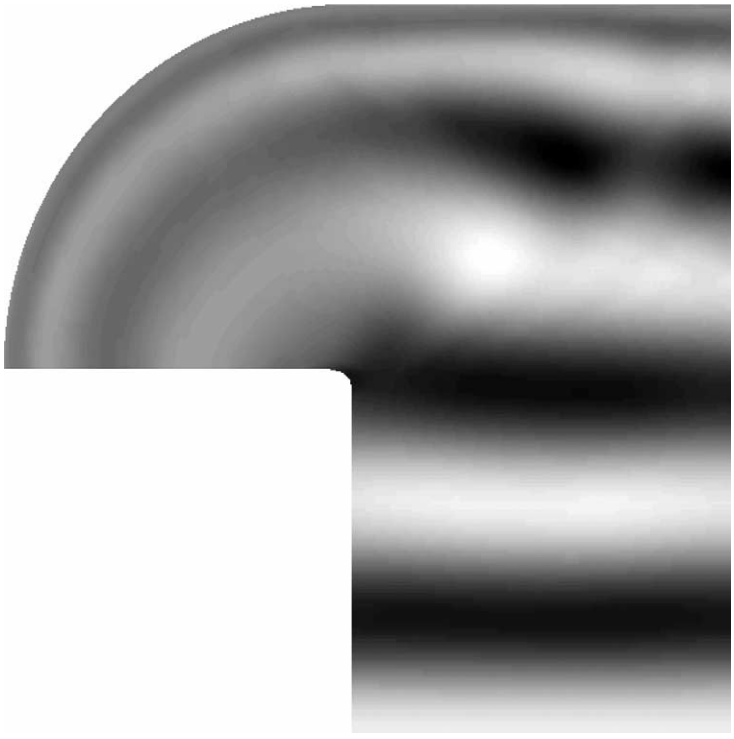

Fig. 14. Wave surface calculated by the present model with wave–current interaction.

instead of the present curvilinear model. In REF/DIF-1, the wet and dry grid technique proposed by Kirby and Dalrymple [10] is used for treating the dry grid points as though they have a very small depth of water (1 mm in the present paper). The results of wave heights calculated from the Cartesian model is shown in Fig. 16. It can be found in the comparison between Figs. 15 and 16 that the Cartesian model obviously underpredicts wave heights in the sheltered region even though the large angle approximation is used in REF/DIF-1.

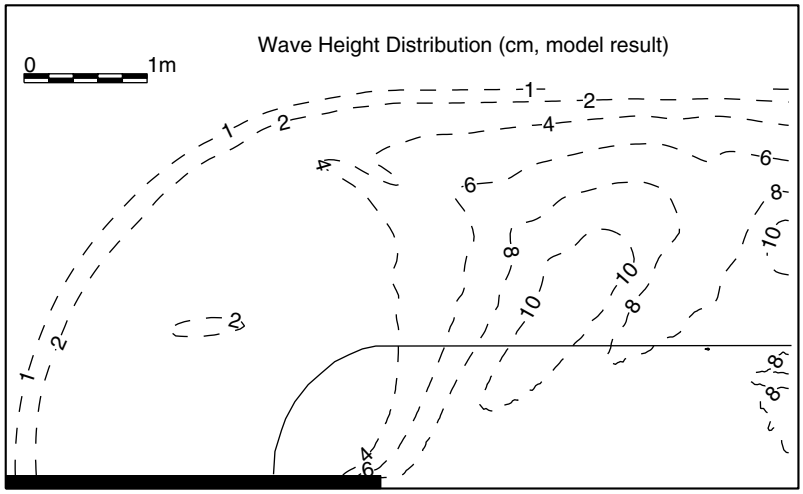

Fig. 15. Wave height calculated by the present model with wave–current interaction.

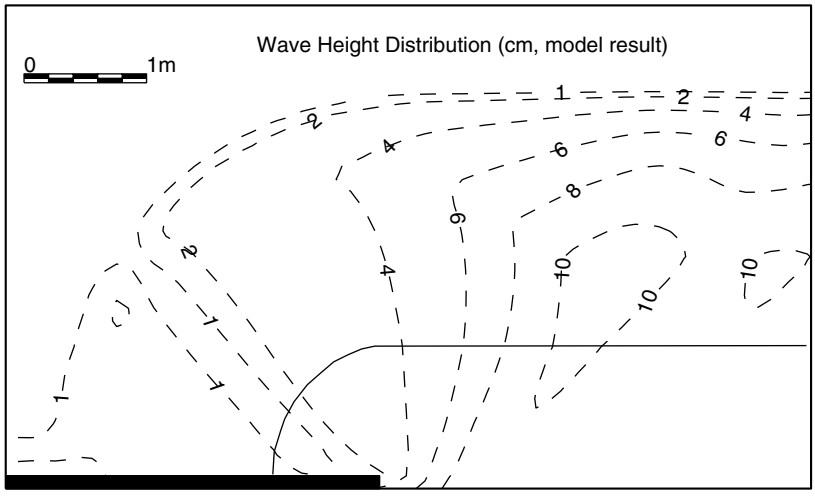

Fig. 16. Wave height calculated by the Cartesian model with wave–current interaction.

5. Conclusions

Covariant/contravariant tensor method is used in the curvilinear parabolic approximation for the vector form of the wave–current equation given by Kirby [8]. The derived model equation can be easily implemented following the model structure and numerical schemes used in the existing code of the Cartesian parabolic model. Besides the curvilinear parabolic approximation, the present model possesses all the features existing in Kirby [8] such as higher-order approximation, wave–current interaction, and treatments of wave breaking and wave non-linearity. The model is then applied to several cases involving curvilinear coordinates in order to examine the curvilinear terms and show model performances. In the first case, the grid stretching terms are verified using analytical solutions of wave propagations in a circular channel. The second case is the calculation of waves propagating into a harbor formed by two diverging breakwaters using non-orthogonal coordinates. The numerical results are compared to Isobe's [6] laboratory measurements and good agreements are obtained. In the last case, the model is used to simulate Gourlay's experiment in order to present the model performance in calculations of wave–current interaction in the complicated domain with a breakwater and a curved beach. Model/data comparisons show that the results with consideration of wave–current interaction agree better than the results without wave–current interaction. Compared to the results from the Cartesian model, the curvilinear model with grid lines tracing principle wave directions can predict better wave diffractions in the sheltered region.

Although the present approach can further improve the calculations of large angle wave propagations, the wave angle limitation caused by the parabolic approximation still exists in model applications. First, the model accuracy depends on a prechosen principal wave direction. In complicated coastal regions, waves propagate in a wide range of directions. Sometimes it is hard to generate a grid that follows multiple principal wave directions. Second, grid distortion may cause a model inaccuracy as mentioned in Section 4.3. In calculations of wave diffractions around coastal structures such as breakwaters, the overbend of grid lines may result in discontinuities of metric tensors which cause numerical errors or instabilities. Such kind of grid needs to be smoothen before using.

Acknowledgments

This study was sponsored by the NOAA Office of Sea Grant, Department of Commerce, under Grant No. NA03OAR4170011 (Project No. R/OE-32). The US Government is authorized to produce and distribute reprints for governmental purposes, not withstanding any copyright notation that may appear hereon. This work was also supported by the National Oceanographic Partnership Program (N00014-99-1-1051).

Appendix A. Booij's splitting method

Using a splitting method, an elliptic equation for $\tilde{\phi}$ can be split into parabolic equations for a forward scattered wave $\tilde{\phi}^+$ and a backward scattered wave $\tilde{\phi}^-$, where

$$\tilde{\phi} = \tilde{\phi}^+ + \tilde{\phi}^- . \tag{A.1}$$

Booij [1] showed that an associated equation

$$(\gamma^{-1}\phi_{m,\xi})_\xi + \gamma\phi_m = 0 \tag{A.2}$$

is split identically into

$$(\phi_m^+)_\xi = \mathrm{i}\gamma\phi_m^+, \tag{A.3}$$

$$(\phi_m^-)_\xi = -\mathrm{i}\gamma\phi_m^-, \tag{A.4}$$

We proceed by defining

$$\phi_m = \alpha\tilde{\phi}, \tag{A.5}$$

which is then substituted into (A.2) to obtain

$$\tilde{\phi}_{\xi\xi} + \frac{\gamma}{\alpha}\left[\alpha(\gamma^{-1})_\xi + \frac{2}{\gamma}\alpha_\xi\right]\tilde{\phi}_\xi + \frac{\gamma}{\alpha}(\gamma^{-1}\alpha_\xi)_\xi\tilde{\phi} + \gamma^2\tilde{\phi} = 0. \tag{A.6}$$

Following Booij [1] and Radder [19], we neglect the derivative of α and reduce (A.6) to

$$\tilde{\phi}_{\xi\xi} + \frac{\gamma}{\alpha}\left[\alpha(\gamma^{-1})_\xi + \frac{2}{\gamma}\alpha_\xi\right]\tilde{\phi}_\xi + \gamma^2\tilde{\phi} = 0. \tag{A.7}$$

Now, we rewrite (26) as

$$\tilde{\phi}_{\xi\xi} + (g^{11}p - U^2)^{-1}(g^{11}p - U^2)_\xi\tilde{\phi}_\xi + k_1^2\left[1 + \frac{M+S}{k_1^2(g^{11}p - U^2)}\right]\tilde{\phi} = 0. \tag{A.8}$$

Comparison with (A.7) leads to the results

$$\gamma = k_1\left[1 + \frac{M+S}{k_1^2(g^{11}p - U^2)}\right]^{1/2}, \tag{A.9}$$

$$\alpha = k_1^{1/2}(g^{11}p - U^2)^{1/2}\left[1 + \frac{M+S}{k_1^2(g^{11}p - U^2)}\right]^{1/4}. \tag{A.10}$$

Substituting (A.9) and (A.10) into (A.3) results in the parabolic equation

$$\begin{aligned}&\frac{\partial}{\partial\xi}\left\{k_1^{1/2}(g^{11}p - U^2)^{1/2}\left[1 + \frac{M+S}{k_1^2(g^{11}p - U^2)}\right]^{1/4}\tilde{\phi}^+\right\}\\ &\quad = \mathrm{i}k_1k_1^{1/2}(g^{11}p - U^2)^{1/2}\left[1 + \frac{M+S}{k_1^2(g^{11}p - U^2)}\right]^{3/4}\tilde{\phi}^+.\end{aligned} \tag{A.11}$$

Approximating the operators in (A.11) using the first two terms of the binomial expansion gives the parabolic model equation (where the + superscript has been dropped)

$$\begin{aligned}&\frac{\partial}{\partial\xi}\left\{k_1^{1/2}(g^{11}p - U^2)^{1/2}\left[1 + \frac{M+S}{4k_1^2(g^{11}p - U^2)}\right]\tilde{\phi}\right\}\\ &\quad = \mathrm{i}k_1k_1^{1/2}(g^{11}p - U^2)^{1/2}\left[1 + \frac{3(M+S)}{4k_1^2(g^{11}p - U^2)}\right]\tilde{\phi}.\end{aligned} \tag{A.12}$$

Denote $k_1(g^{11}p - U^2) = \delta$. Then, (A.12) may be written as

$$\frac{\partial}{\partial\xi}(\delta^{1/2}\tilde{\phi}) + \frac{\partial}{\partial\xi}\left(\frac{R}{4k_1\delta^{1/2}}\tilde{\phi}\right) = \mathrm{i}k_1\delta^{1/2}\tilde{\phi} + \mathrm{i}\frac{3R}{4\delta^{1/2}}\tilde{\phi}. \tag{A.13}$$

Denote $R\tilde{\phi} = M'\tilde{\phi} + N\tilde{\phi} + S\tilde{\phi}$, where $N\tilde{\phi}$ are the localized non-linear and dissipation terms and $S\tilde{\phi}$ is expressed in (28). Then

$$M'\tilde{\phi} = \left\{2\omega k_1 U + \mathrm{i}\omega\frac{1}{J}[(JU)_\xi + (JV)_\eta]\right\}\tilde{\phi} - (UV\tilde{\phi}_\eta)_\xi - (UV\tilde{\phi}_\xi)_\eta + \left[(g^{22}p - V^2)\tilde{\phi}_\eta\right]_\eta + 2\mathrm{i}\omega(U\tilde{\phi}_\xi + V\tilde{\phi}_\eta), \tag{A.14}$$

$$N\tilde{\phi} = -\sigma^2 k_1^2 g^{11} D|A|^2\tilde{\phi} - \mathrm{i}\sigma\frac{w}{2}\tilde{\phi}. \tag{A.15}$$

We will use a local phase and amplitude according to

$$\tilde{\phi} = -\mathrm{i}g\left(\frac{A'}{\sigma}\right)\mathrm{e}^{\mathrm{i}\psi}; \quad \psi = \int k_1(\xi,\eta)\,\mathrm{d}\xi - \omega t, \tag{A.16}$$

so that

$$\frac{\partial\tilde{\phi}}{\partial\xi} = -\mathrm{i}g\left[\left(\frac{A'}{\sigma}\right)_\xi + \mathrm{i}k_1\left(\frac{A'}{\sigma}\right)\right]\mathrm{e}^{\mathrm{i}\psi} \simeq \mathrm{i}k_1\tilde{\phi} \quad \text{at lowest} - \text{order}. \tag{A.17}$$

After dropping some small terms such as $\frac{\partial k_1}{\partial\xi}/k_1^2 N\tilde{\phi}$ and $\frac{\partial k_1}{\partial\xi}/k_1^2 S\tilde{\phi}$ and using lowest-order

$$N\tilde{\phi}_\xi = \mathrm{i}k_1 N\tilde{\phi}, \tag{A.18}$$

$$S\tilde{\phi}_\xi = \mathrm{i}k_1 S\tilde{\phi}. \tag{A.19}$$

Eq. (A.13) may be written as

$$\delta\frac{\partial\tilde{\phi}}{\partial\xi} + \frac{1}{2}\frac{\partial\delta}{\partial\xi}\tilde{\phi} - \mathrm{i}k_1\delta\tilde{\phi} - \frac{\mathrm{i}}{2}(N+S)\tilde{\phi} + \frac{1}{4k_1}(M\tilde{\phi})_\xi - \frac{3\mathrm{i}}{4}(M\tilde{\phi}) - \frac{1}{4}\beta(M\tilde{\phi}) = 0, \tag{A.20}$$

where β is given by (31). Notice that

$$\delta = k_1(g^{11}p - U^2) = \sigma(\sqrt{g^{11}}C_\mathrm{g} + U) - \omega U. \tag{A.21}$$

Eq. (A.20) can be rewritten as (30) using (A.21).

Appendix B. Model equation from cartesian parabolic approximation [8]

Starting with the time-dependent wave–current equation (1), Kirby [8] derived the following higher-order parabolic equation in the Cartesian coordinate system (x,y), assuming that waves propagate dominantly in the x-direction.

$$\begin{aligned}
&(C_\mathrm{g}+u)A_x + vA_y + \mathrm{i}(\bar{k}-k)(C_\mathrm{g}+u)A + \frac{\sigma}{2}\left[\left(\frac{C_\mathrm{g}+u}{\sigma}\right)_x + \left(\frac{v}{\sigma}\right)_y\right]A - \frac{\mathrm{i}}{2}\left[(p-v^2)\left(\frac{A}{\sigma}\right)_y\right]_y \\
&+ \frac{\mathrm{i}}{2}\left\{\left[uv\left(\frac{A}{\sigma}\right)_y\right]_x + \left[uv\left(\frac{A}{\sigma}\right)_x\right]_y\right\} + \frac{\mathrm{i}\sigma}{2}k^2 D|A|^2 A + \frac{w}{2}A + \frac{1}{4k}\left\{\left[(p-v^2)\left(\frac{A}{\sigma}\right)_y\right]_{yx} + 2\mathrm{i}\left[\sigma v\left(\frac{A}{\sigma}\right)_y\right]_x\right\} \\
&+ \frac{\beta}{4}\left\{2\mathrm{i}\omega u\left(\frac{A}{\sigma}\right)_x + 2\mathrm{i}\sigma v\left(\frac{A}{\sigma}\right)_y - 2uv\left(\frac{A}{\sigma}\right)_{xy} + \left[(p-v^2)\left(\frac{A}{\sigma}\right)_y\right]_y\right\} \\
&+ \frac{\mathrm{i}}{4k}[(\omega v)_y + 3(\omega u)_x]\left(\frac{A}{\sigma}\right)_x + S' = 0.
\end{aligned} \tag{B.1}$$

References

[1] N. Booij, Gravity Waves on Water with Non-uniform Depth and Current, Rep 81-1, Department of Civil Engineering, Delft Univeristy of Technology, Delft, 1981.
[2] J.U. Brackbill, J.S. Saltzman, Adaptive zoning for singular problems in two dimensions, J. Comput. Phys. 46 (1982) 342–368.
[3] R.A. Dalrymple, J.T. Kirby, P.A. Hwang, Wave diffraction due to areas of energy dissipation, J. Waterway, Port, Coastal Ocean Eng. 110 (1984) 67–79.
[4] R.A. Dalrymple, J.T. Kirby, P.A. Martin, Spectral methods for forward-propagating water waves in conformally-mapped channels, Appl. Ocean Res. 16 (1994) 249–266.
[5] M.R. Gourlay, Wave set-up and wave generated currents in the lee of a breakwater or headland, in: Proceedings of the 14th Coastal Engineering Conference, Copenhagen, 1974, pp. 1976–1995.
[6] M. Isobe, A parabolic refraction-diffraction equation in the ray-front coordinate system, in: Proceedings of the 20th International Conference on Coastal Engineering, Taipei, 1986, pp. 306–317.
[7] J.T. Kirby, R.A. Dalrymple, A parabolic equation for the combined refraction-diffraction of Stokes waves by mildly-varying topography, J. Fluid Mech. 136 (1983) 453–466.
[8] J.T. Kirby, Higher-order approximations in the parabolic equation method for water waves, J. Geophys. Res. 91 (1986) 933–952.
[9] J.T. Kirby, R.A. Dalrymple, An approximate model for nonlinear dispersion in monochromatic wave propagation models, Coastal Eng. 9 (1986) 545–561.
[10] J.T. Kirby, R.A. Dalrymple, Modeling waves in surfzones and around islands, J. Waterway, Port, Coastal Ocean Eng. 112 (1986) 78–93.
[11] J.T. Kirby, Parabolic wave computations in non-orthogonal coordinate systems, J. Waterway, Port, Coastal Ocean Eng. 114 (1988) 673–685.
[12] J.T. Kirby, R.A. Dalrymple, H. Kaku, Parabolic approximations for water waves in conformal coordinate systems, Coastal Eng. 23 (1994) 185–213.
[13] J.T. Kirby, R.A. Dalrymple, F. Shi, Combined Refraction/Diffraction Model REF/DIF 1, Version 2.6. Documentation and User's Manual, Research Report, Center for Applied Coastal Research, Department of Civil and Environmental Engineering, University of Delaware, Newark, 2004.
[14] P.L.-F. Liu, Viscous effects on evolution of Stokes waves, J. Waterway, Port, Coastal Ocean Eng. 112 (1) (1986) 55–63.
[15] P.L.-F. Liu, P. Boissevain, Wave propagation between two breakwater, J. Waterway, Port, Coastal Ocean Eng. 114 (2) (1988) 237–347.
[16] F. Shi, I.A. Svendsen, J.T. Kirby, J.M. Smith, A curvilinear version of a quasi-3D nearshore circulation model, Coastal Eng. 49 (2003) 99–124.
[17] T.-K. Tsay, P.L.-F. Liu, Numerical solution of water wave refraction and diffraction problems in the parabolic approximation, J. Geophys. Res. 87 (1982) 7932–7940.
[18] T.-K. Tsay, B.A. Ebersole, P.L.-F. Liu, Numerical modelling of wave propagation using parabolic approximation with a boundary-fitted co-ordinate system, Int. J. Numer. Meth. Fluids 27 (1989) 37–55.
[19] A.C. Radder, On the parabolic equation method for water wave propagation, J. Fluid Mech. 72 (1979) 373–384.